DOI: 10.1021/cg100236c

CRYSTAL GROWTH & DESIGN Article

2010, Vol. 10
3110–3119

Two-Dimensional Polyoxoniobates Constructed from Lindqvist-Type Hexaniobates Functionalized by Mixed Ligands

Jingyang Niu,* Xiao Fu, Junwei Zhao, Suzhi Li, Pengtao Ma, and Jingping Wang*

Institute of Molecular and Crystal Engineering, College of Chemistry and Chemical Engineering, Henan University, Kaifeng, Henan 475004, P. R. China

Received February 19, 2010; Revised Manuscript Received May 17, 2010

ABSTRACT: By introducing mixed ligands into the hexaniobate system, three novel organic−inorganic hybrids, $[Cu(en)_2]_2\{[Cu(1,10\text{-phen})][Cu(1,10\text{-phen})(H_2O)]Nb_6O_{19}\}\cdot 10.5H_2O$ (**1**), $[Cu(en)_2]_2\{[Cu(2,2'\text{-bipy})][Cu(2,2'\text{-bipy})(H_2O)]Nb_6O_{19}\}\cdot 9H_2O$ (**2**) and $[Cu(1,2\text{-dap})_2]_2\{[Cu(2,2'\text{-bipy})][Cu(2,2'\text{-bipy})(H_2O)]Nb_6O_{19}\}\cdot 11H_2O$ (**3**) (en = ethylenediamine, 1,10-phen = 1,10-phenanthroline, 2,2′-bipy = 2,2′-bipydine, 1,2-dap = 1,2-diaminopropane), have been synthesized by the solution diffusion method and characterized by elemental analyses, IR spectra, UV spectroscopy, thermogravimetric analyses, and single-crystal X-ray diffraction. **1**, **2**, and **3** can be formularized as $[Cu(L_1)_2]_2\{[Cu(L_2)][Cu(L_2)(H_2O)]Nb_6O_{19}\}\cdot nH_2O$ (L_1 = en for **1** and **2**, 1,2-dap for **3**, L_2 = 1,10-phen for **1**, 2,2′-bipy for **2** and **3**, n = 10.5 for **1**, 9 for **2**, 11 for **3**), and all exhibit the two-dimensional (2D) network architecture built by $[Cu(L_1)_2]_2\{[Cu(L_2)][Cu(L_2)(H_2O)]Nb_6O_{19}\}$ units and $[Cu(L_1)_2]^{2+}$ bridges. **1**−**3** represent the first 2D architecture with (4,4)-connected topology in polyoxoniobate chemistry. Furthermore, the photoluminescent properties of **1** and **2** have been studied. The magnetic behavior of **1** has been quantitatively investigated and suggests the weak antiferromagnetic exchange interactions.

Introduction

Polyoxometalates (POMs), anionic metal-oxide clusters with an unmatched range of physical and chemical properties, have been employed as attractive building blocks to construct larger clusters or fascinating one-, two-, and three-dimensional (1D, 2D, and 3D) extended structures.[1] This fact stems not only from their unique architectures but also from their wide applications as diverse as catalysis, electrical conductivity, photochemistry, medicine, and magnetism.[2,3] Some achievements in this aspect have been made with persistent efforts. For example, in 2000, Pope et al. first reported two 1D Ln-substituted monovacant Keggin silicotungstates $[Ln(\alpha\text{-}SiW_{11}O_{39})(H_2O)_3]^{5-}$ ($Ln = La^{III}$, Ce^{III}).[1d] In 2001, Zubieta et al. isolated a novel 2D polyoxomolybdate with organophosphorous ligands $[\{Cu_2(tpypyz)(H_2O)_2\}(Mo_5O_{15})(O_3PCH_2CH_2PO_3)]\cdot 5.5\ H_2O$ [tpypyz = tetra(2-pyridyl)pyrazine].[1e] In 2006, Wang et al. reported an unprecedented (4,12)-connected 3D phosphomolybdate $(NH_4)[Cu_{24}I_{10}L_{12}][PMo^{V}_{2}Mo^{VI}_{10}\ O_{40}]_3$ [L = 4-[3-(1H-1,2, 4-triazol-1-yl)propyl]-4H-1,2,4-triazole] assembled by nanometer-scale $[Cu_{24}I_{10}L_{12}]^{14+}$ clusters and ball-shaped Keggin $[PMo^{V}_{2}Mo^{VI}_{10}O_{40}]^{5-}$ anions.[1f]

In comparison with polyoxovanadates, -molybdates, and -tungstates, the research on polyoxoniobates (PONs) is very limited, although the Lindqvist-type hexaniobate anion $[Nb_6O_{19}]^{8-}$ was first structurally described in 1953.[4] This fact may be due to the difficulty in synthesis controlling and the narrow working pH range (10.5−12.5) of PONs.[5,6] Some typical examples are as follows: in 1969, two sandwich-type Lindqvist dimers $[M(Nb_6O_{19})_2]^{12-}$ [(M = Mn^{IV}, Ni^{IV}] were reported.[7] In 1977, Graeber and Morosin isolated an isopolyoxoniobate $[Nb_{10}O_{28}]^{6-}$.[8] In 1994, Yamase et al. synthesized a large composite PONs $\{[Eu_3O(OH)_3(OH_2)_3]_2Al_2(Nb_6O_{19})_5\}^{26-}$ constructed from five $[Nb_6O_{19}]^{8-}$ anions linked by two trimeric europium clusters and two Al^{3+} cations.[9] Since 2000, increasing interest in PONs has been further triggered because of their potential applications in virology, nuclear-waste treatment, and the base-catalyzed decomposition of biocontaminants.[10,11] In 2001, Pope et al. separated several hexaniobate carbonyl derivatives $[Nb_6O_{19}\{M(CO)_3\}_n]^{(8-n)-}$ (M = Mn^{I}, Re^{I}; n = 1, 2).[11] In the following year, two hybrid PONs $\{trans/cis\text{-}[H_xNb_6O_{19}][Ni^{II}(taci)]_2\}^{n-}$ [(taci = 1,3,5-triamino-1,3,5-trideoxy-*cis*-inositol), x = 0, n = 4 and x = 2, n = 2] were prepared under solvothermal conditions.[12] In this field, Nyman's group made great contributions: in 2002, they synthesized a Keggin-type heteropolyniobate $[SiNb_{12}\ O_{40}]^{16-}$ and its lacunary derivative $[H_2Si_4Nb_{16}O_{56}]^{14-}$ under hydrothermal conditions.[13a] Later, a class of Keggin-type silico- and germano-dodecaniobates, such as $[GeNb_{12}O_{40}]^{16-}$,[13b] $Na_{12}[Ti_2O_2][TNb_{12}O_{40}]\cdot xH_2O$,[13c] and $Na_{10}[Nb_2O_2][TNb_{12}O_{40}]\cdot xH_2O$ [T = Si^{IV}, Ge^{IV}] were obtained.[13c] In 2006, a novel isopolyniobate $[Nb_{24}O_{72}H_9]^{15-}$ was communicated.[5] Meanwhile, they first prepared a trivacant α-Keggin anion $[(PO_2)_3PNb_9O_{34}]^{15-}$.[14] In addition, a novel icosaniobate $[Nb_{20}O_{54}]^{8-}$ was reported in 2006.[15] Subsequently, Nyman's group published five organic−inorganic hybrids containing $[Nb_6O_{19}]^{8-}$ clusters: $[(Nb_6O_{19}H_2)_2Cu(en)_2]^{10-}$, $[(Nb_6O_{19}H_2)Cu(en)_2]^{4-}$, $\{[Nb_6O_{19}][Cu(NH_3)]_2\}_2^{8-}$, $\{[Nb_6O_{19}][Cu(NH_3)_2(H_2O)]_2[Cu(H_2O)_4]_2\}\cdot 3H_2O$, and $\{[Nb_6O_{19}][Cu(NH_3)_2(H_2O)]_2[Cu(H_2O)_4]_2\}$.[16] Recently, Casey et al. illustrated a new polyoxotitanoniobate $[Ti_{12}Nb_6O_{44}]^{10-}$ consisting of a cubic $[Ti_{12}O_{14}]^{20+}$ core.[17] More recently, Cronin et al. discovered the largest isopolyoxoniobaters $[HNb_{27}O_{76}]^{16-}$ and $[H_{10}Nb_{31}O_{93}\ (CO_3)]^{23-}$ in the presence of sodium dibenzyldithiocarbamate.[6]

Obviously, most of the previously reported PONs are purely inorganic compounds. Therefore, it remains a great opportunity and challenge for exploring and discovering organic−inorganic hybrid PONs. Since 2005, our group has concentrated on the reactivity of hexaniobates with transition-metal complexes. In 2007, we successfully obtained a family of organic−inorganic hybrid PONs $[(\{KNb_{24}O_{72}H_{10.25}\}\{Cu(en)_2\})_2\{Cu_3(en)_3(H_2O)_3\}\{Na_{1.5}Cu_{1.5}(H_2O)_8\}]^{11-}$, $[H_{23}NaO_8Cu_{24}(Nb_7O_{22})_8]^{16-}$, and $[H_9Cu_{25.5}O_8(Nb_7O_{22})_8]^{28-}$.[18] Later, we employed the aromatic ligand 2,2′-bipy instead of the aliphatic diamine ligand en to prepare a novel organic−inorganic hybrid PON

*To whom correspondence should be addressed. E-mail: jpwang@henu.edu.cn. Fax: (+86) 378 3886876.

 Published on Web 06/03/2010

$\{Nb_6O_{19}[Cu(2,2'\text{-bipy})]_2[Cu(2,2'\text{-bipy})_2]_2\}\cdot 19H_2O$.[19] Additionally, Hu et al. also isolated two isostructural 1D hybrid decaniobates $\{[M(2,2'\text{-bipy})_2]_3[Nb_{10}O_{28}]\cdot XH_2O\}_n$ (M = Zn^{II} and Co^{II}, X = 3 and 1.5).[20] These reported organic−inorganic hybrid PONs only contain a type of organic ligand; however, the Lindqvist-type hexaniobates containing mixed organic ligands have never been reported so far. In this context, we simultaneously employ aromatic N-ligands such as 2,2′-bipy or 1,10-phen and aliphatic diamine ligands such as en or 1,2-dap to prepare novel Lindqvist-type hexaniobates with mixed organic ligands. Fortunately, by trial and error, we have obtained three novel organic−inorganic hybrid hexaniobates: $[Cu(en)_2]_2\{[Cu(1,10\text{-phen})][Cu(1,10\text{-phen})(H_2O)]Nb_6O_{19}\}\cdot 10.5H_2O$ (**1**), $[Cu(en)_2]_2\{[Cu(2,2'\text{-bipy})][Cu(2,2'\text{-bipy})(H_2O)]Nb_6O_{19}\}\cdot 9H_2O$ (**2**), and $[Cu(1,2\text{-dap})_2]_2\{[Cu(2,2'\text{-bipy})][Cu(2,2'\text{-bipy})(H_2O)]Nb_6O_{19}\}\cdot 11H_2O$ (**3**). **1**, **2**, and **3** can be formularized as $[Cu(L_1)_2]_2\{[Cu(L_2)][Cu(L_2)(H_2O)]Nb_6O_{19}\}\cdot nH_2O$ (L_1 = en for **1** and **2**, 1,2-dap for **3**, L_2 = 1,10-phen for **1**, 2,2′-bipy for **2** and **3**, n = 10.5 for **1**, **9** for **2**, 11 for **3**). The common structural feature is that all display the 2D network constructed from $[Cu(L_1)_2]_2\{[Cu(L_2)][Cu(L_2)(H_2O)]Nb_6O_{19}\}$ units and $[Cu(L_1)_2]^{2+}$ bridges. To our knowledge, **1**−**3** represent the first 2D architecture with (4,4)-connected topology in PON chemistry. Furthermore, the photoluminescence properties of **1** and **2** were studied. The magnetic behavior for **1** was quantitatively analyzed.

Experimental Section

General Methods and Materials. All chemicals were commercially purchased and used without further purification. $K_7HNb_6O_{19}\cdot 13H_2O$ was synthesized according to the literature[21] and characterized by IR spectrum. Elemental analyses (C, H, N) were performed on a Perkin-Elmer 2400 CHN elemental analyzer; IR spectra were obtained in the range of 4000−400 cm^{-1} on a Nicolet 170 SXFT-IR spectrometer with pressed KBr pellets. Thermogravimetric (TG) analyses were performed on a Mettler-Toledo TGA/SDTA 851^e thermal analyzer in a flowing air atmosphere in the temperature region of 25−800 °C with a heating rate of 10 °C·min^{-1}. X-ray powder diffraction (XRPD) measurements were performed on a Philips X'Pert-MPD instrument with Cu Kα radiation (λ = 1.54056 Å) in the angular range 2θ = 10−40° at 293 K. Emission/excitation spectra were recorded on an F-7000 fluorescence spectrophotometer. UV absorption spectra were obtained with a U-4100 spectrometer at room temperature. Magnetic susceptibility measurements were obtained by the use of a Quantum Design MPMS-XL7 SQUID magnetometer at a temperature ranging from 2 to 300 K.

Synthesis of 1. $K_7HNb_6O_{19}\cdot 13H_2O$ (0.34 g, 0.25 mmol) was dissolved in 50 mL of water, and then a 20 mL aqueous solution containing 1,10-phen (0.20 g, 1.00 mmol), en (0.80 mL, 0.50 mmol), and $Cu(CH_3COO)_2\cdot H_2O$ (0.20 g, 1.00 mmol) was slowly added with stirring at 55 °C for 6 h. The resulting mixture was cooled to room temperature and filtered. The blue filtrate was transferred to a straight glass tube, and a mixed solvent of CH_3CH_2OH/H_2O (2:3, volume ratio) was carefully layered onto the blue filtrate. Block-shaped dark blue crystals of **1** appeared at the interface after 13 days. Yield: ca. 22% (based on $K_7HNb_6O_{19}\cdot 13H_2O$). Anal. Calcd. (found %) for $C_{32}H_{71}Cu_4N_{12}Nb_6O_{30.50}$ (**1**): C 19.98 (19.85), H 3.72 (3.81), N 8.74 (8.84). IR (KBr pellet): 3390(s), 3324(s), 3235(s), 1627(m), 1584(m), 1518(m), 1459(w), 1429(m), 1398(w), 1149(w), 1045 (m), 854(s), 726(s), 683(s), 528(s), 415(s).

Synthesis of 2. $K_7HNb_6O_{19}\cdot 13H_2O$ (0.69 g, 0.50 mmol) was dissolved in a 50 mL aqueous solution, and then a 21 mL aqueous solution containing 2,2′-bipy (0.22 g, 1.40 mmol), en (1.40 mL, 0.50 mmol), and $Cu(CH_3COO)_2\cdot H_2O$ (0.24 g, 1.20 mmol) was slowly added with stirring at 60 °C for 6 h. The resulting mixture was cooled to room temperature and filtered. The dark green filtrate was transferred to a straight glass tube, and a mixed solvent of CH_3CH_2OH/H_2O (2:3, volume ratio) was carefully layered onto the dark green solution. Block-shaped dark blue crystals of **2** appeared at the interface after 15 days. Yield: ca. 24% (based on $K_7HNb_6O_{19}\cdot 13H_2O$). Anal. Calcd. (found %) for $C_{28}H_{68}Cu_4N_{12}Nb_6O_{29}$ (**2**): C 18.19 (18.07), H 3.71 (3.78), N 9.09 (8.96); IR (KBr pellet): 3379(s), 3299(s), 3138(s), 1604(m), 1495(m), 1472(m), 1448(m), 1313(w), 1165 (w), 1111(w), 851(s), 773(s), 731(s), 680(s), 527(s), 409(s).

Synthesis of 3. The procedure for the formation of **1** was employed, but instead of a 20 mL aqueous solution containing 1,10-phen (0.20 g, 1 mmol), en (0.80 mL, 0.50 mmol), and $Cu(CH_3COO)_2\cdot H_2O$ (0.20 g, 1.00 mmol) we used a 20 mL aqueous solution containing 2,2′-bipy (0.38 g, 2.40 mmol), 1,2-dap (4.80 mL, 0.50 mmol), and $Cu(CH_3COO)_2\cdot H_2O$ (0.20 g, 1.00 mmol). Yield: ca. 31% (based on $K_7HNb_6O_{19}\cdot 13H_2O$). Anal. Calcd. (found %) for $C_{32}H_{80}Cu_4N_{12}Nb_6O_{31}$ (**3**): C 19.80 (19.67), H 4.16 (4.25), N 8.66 (8.72); IR (KBr pellet): 3400(s), 3258(s), 3134(s), 2967(s), 1602(s), 1498(m), 1482(m), 1446(m), 1387(w), 1382(w), 1321(w), 1161 (m), 1095 (w), 1064 (m), 1029(m), 858(s), 775(s), 734 (s), 679(s), 534(s), 408(s).

X-ray Crystallography. A dark blue block crystal with dimensions of 0.41 × 0.22 × 0.14 mm^3 for **1**, 0.487 × 0.263 × 0.272 mm^3 for **2**, and 0.410 × 0.223 × 0.139 mm^3 for **3** was mounted on a glass fiber. Intensity data were collected on Bruker APEX-II CCD detector at 296(2) K with Mo Kα radiation (λ = 0.71073 Å). The structures were solved by direct methods using the SHELXTL-97 program[22] and refined by full-matrix least-squares on F^2 using the SHELXTL-97 program package. Lorentz polarization and empirical absorption corrections were applied. All the non-hydrogen atoms were refined anisotropically. All the hydrogen atoms were placed in idealized positions and refined with a riding model using default SHELXL parameters. Those hydrogen atoms attached to lattice water molecules were not located. Crystallographic data and structure refinements for **1**−**3** were summarized in Table 1. CCDC reference nos. 764381, 764382, and 764383 for **1**, **2**, and **3**, respectively. The data of **1**−**3** can be obtained free of charge from The Cambridge Crystallographic Data Centre via www. ccdc.cam.ac.uk/data_request/cif.

Table 1. Crystallographic Data and Structural Refinements for 1−3

	1	2	3
formula	$C_{32}H_{71}Cu_4N_{12}Nb_6O_{30\ 5}$	$C_{28}H_{68}Cu_4N_{12}Nb_6O_{29}$	$C_{32}H_{80}Cu_4N_{12}Nb_6O_{31}$
M_r (g mol^{-1})	1923.59	1848.52	1940.66
T (K)	296(2)	296(2)	296(2)
space group	$P2(1)2(1)2$	$Pnnm$	$Pnnm$
crystal system	orthorhombic	orthorhombic	orthorhombic
a (Å)	31.045(2)	30.8690(15)	31.9429(18)
b (Å)	13.9893(11)	13.7091(6)	13.6686(8)
c (Å)	14.4513(11)	14.6688(7)	14.6214(8)
V ($Å^3$)	6276.2(8)	6207.6(5)	6383.9(6)
Z	4	4	4
D_c (g cm^{-3})	2.036	1.959	1.978
μ (mm^{-1})	2.469	2.488	2.426
limiting indices	$-36 \le h \le 36$	$-36 \le h \le 30$	$-37 \le h \le 37$
	$-16 \le k \le 16$	$-15 \le k \le 16$	$-16 \le k \le 16$
	$-17 \le l \le 14$	$-17 \le l \le 17$	$-13 \le l \le 17$
GOF on F^2	1.077	1.086	1.070
R_1, wR_2 [$I > 2\sigma(I)$]	0.0286, 0.0717	0.0465, 0.1310	0.0834, 0.1987
R_1, wR_2 [all data]	0.0338, 0.0737	0.0526, 0.1343	0.1004, 0.2058

Results and Discussion

Synthesis. In recent years, several organic−inorganic hybrid PONs have been successfully obtained by virtue of the conventional solvent evaporation methods. Table 2 shows the formation conditions of some hybrid PONs in the presence of en or 2,2′-bipy. Following the analogous approach, en was replaced by 1,2-dap/1,3-dap/deta/teta (1,3-dap = 1,3-diaminopropane, deta = diethylenetriamine, teta = triethylenetetramine), but all attempts failed. We conjecture that the key factor may be intimately related to the coordination capability and flexible geometric configuration of en ligands. On the other hand, the interaction of en with Cu^{II} ions can lead to $[Cu(en)_x]^{2+}$ complexes and enhance the stability of Cu^{II} ions in an

Table 2. Summary of Synthetic Conditions and Related Phases in the Preparations of 1−3

reactant and molar ratio	*T* (°C)	synthetic method	dimension	phase
$K_7HNb_6O_{19}/Cu^{2+}$/en/1,10-phen = 1/ 2.4/1.6/2.4	55	solution diffusion	2D	**1**
$K_7HNb_6O_{19}/Cu^{2+}$/en/2,2′-bipy = 1/3/0.88/1.76	60	solution diffusion	2D	**2**
$K_7HNb_6O_{19}/Cu^{2+}$/1,2-dap/2,2′-bipy = 1/2/4/4	55	solution diffusion	2D	**3**
$Rb_8Nb_6O_{19}/Cu^{2+}$/en = 1/ 4/334	60	solvent evaporation	dimer	$[(\{Nb_{24}O_{72}H_9\}\{Cu(en)_2(H_2O)\}_2\{Cu(en)_2\})_2]\cdot 18H_2O$[5]
$Rb_8Nb_6O_{19}/Cu^{2+}$/en = 1/3.9/136.4	60	solvent evaporation	dimer	$[(Nb_6O_{19}H_2)_2Cu(en)_2]$[10−16]
$Rb_8Nb_6O_{19}/Cu^{2+}$/en = 1/ 7.8/272.7	60	solvent evaporation	1D	$[(Nb_6O_{19}H_2)Cu(en)_2]$[4−16]
$K_7HNb_6O_{19}/Cu^{2+}$/2,2′-bipy = 1/4/8	60	solvent evaporation	0D	$\{Nb_6O_{19}[Cu(2,2'\text{-bipy})]_2[Cu(2,2'\text{-bipy})_2]_2\}\cdot 19H_2O$[19]
$K_7HNb_6O_{19}/Zn^{2+}$/2,2′-bipy/ $Na_2S_2O_3\cdot 6H_2O$ = 1/3/6.1/6.1	100	hydrothermal conditions	1D	$\{[Zn(2,2'\text{-bipy})_2]_3[Nb_{10}O_{28}]\cdot 3H_2O\}_n$[20]
$K_7HNb_6O_{19}/Co^{2+}$/2,2′-bipy/ $Na_2S_2O_3\cdot 6H_2O$ = 1/3/6.1/6.1	100	hydrothermal conditions	1D	$\{[Co(2,2'\text{-bipy})_2]_3[Nb_{10}O_{28}]\cdot 1.5H_2O\}_n$[20]

alkaline hexaniobate system. These elucidate that organoamines play an important tunable role in the formation and structural construction of PONs.

Considering the similarity in structure between 1,10-phen and 2,2′-bipy, when 1,10-phen was employed, a novel 1,10-phen-containing PON $\{[Cu(1,10\text{-phen})(H_2O)]_2Cu[Nb_{11}O_{35}H_4]\}^{5-}$ was obtained by the solution diffusion method.[23] When 1,10-phen was replaced by 4,4′-bipy, only amorphous powders were afforded. In addition, if H_2biim (H_2biim = 2,2′-biimdazole) was used, the cube-shaped PON $K_{16}Na_{12}[H_9Cu_{25.5}O_8(Nb_7O_{22})_8]\cdot 73.5H_2O$ was afforded.[18] We believe that the rigid and steric hindrance of 4,4′-bipy and H_2biim affect the formation of organic−inorganic hybrid PONs.

These intriguing results ignited and spurred on our intensive interest. To the best of our knowledge, no investigation on the PONs with mixed organic ligands was carried out. Thus, we intended to introduce aliphatic N-ligands (en or 1,2-dap) and aromatic N-ligands (2,2′-bipy or 1,10-phen) to one reaction system to construct organic−inorganic hybrid PONs. Under the guidance of this concept, the hexaniobate anion $[Nb_6O_{19}]^{8-}$ is employed chiefly due to its high negative charge surface, rich surface oxygen atoms, and high stability under basic conditions (pH > 10), which may provide the possibility of constructing novel multidimensional architectures.[16,24] At the beginning, the reaction of the hexaniobate anion $[Nb_6O_{19}]^{8-}$ with the Cu^{II} ion in the presence of 2,2′-bipy and en resulted in the first organic−inorganic hybrid hexaniobate $[Cu(en)_2]_2\{[Cu(2,2'\text{-bipy})][Cu(2,2'\text{-bipy})(H_2O)]Nb_6O_{19}\}\cdot 9H_2O$ (**2**) with mixed ligands. When 1,2-dap repalced en, as expected, **3** was obtained, which is isostructural to **2**. Following this strategy, we harvested **1** when 2,2′-bipy was replaced by 1,10-phen. Finally, it was found that **1** was obtained only in a limited range between 55 and 60 °C while **2** and **3** can be formed in the range of 55−70 °C. When 1,2-dap and 1,10-phen were employed, a reported giant cube-shaped PON $K_{16}Na_{12}[H_9Cu_{25.5}O_8(Nb_7O_{22})_8]\cdot 73.5H_2O$ was obtained.[18] The reason may be that the steric hindrance of 1,2-dap/1,10-phen is larger than those of en/2,2′-bipy and 1,2-dap/2,2′-bipy, leading to the separation between metal−organic units and hexaniobate anions.[25]

During the course of our exploration, we found that it was more difficult to control the syntheses of products with mixed ligands than those with single ligands. This is mainly attributed to the fact that mixed organic ligands have different solubilities as well as different binding capabilities for transition-metal ions. We also investigated the reaction of other transition-metal ions (Co^{II}, Ni^{II}, and Mn^{II}) with hexaniobate anion $[Nb_6O_{19}]^{8-}$ in the participation of mixed ligands, unfortunately, no analogous hexaniobates were obtained. One reason may be related to the fact that the d^9 Cu^{II} ion has flexible coordination modes and obvious Jahn−Teller distortion,[26] and another important reason is the affinity of Cu^{II} ions for these family of ligands. These indicate that the nature of transition metal ions has a decisive influence on the formation of the products.

Table 3. Selected Bond Lengths [Å] for 1−3

A−X	1	2	3
Nb═O	1.761(4)−1.784(4)	1.766(4)−1.785(5)	1.771(7)−1.789(7)
Nb−O	1.922(3)−2.101(3)	1.914(3)−2.089(3)	1.929(7)−2.102(7)
Nb−$O_{\mu 6}$	2.345(3)−2.417(3)	2.354(3)−2.397(4)	2.364(6)−2.412(9)
Cu−N	2.000(5)−2.037(5)	1.979(6)−2.020(7)	1.937(2)−2.410(3)
Cu−O_{Nb6O19}	1.950(3)−3.006(3)	1.965(3)−2.736(3)	1.961(7)−2.732(8)
Cu−Ow	2.860(6)	2.969(1)	2.982(2)

It is noted that the isolation of **1**−**3** illustrates that the solution diffusion approach is efficient and feasible in the preparation of novel PONs with mixed ligands. This approach is relatively straightforward via layering the ethanol−water solution on the aqueous solution of transition-metal complexes and $K_7HNb_6O_{19}\cdot 13H_2O$. With the slow diffusion of solution, the dark blue crystals of **1**−**3** formed at interfaces. However, this approach still needs to be further explored, because many factors (the categories and ratios of solvent, the pH of the solution, the concentration of the reaction mixture, etc.) can affect the formation of crystal phases: (i) We need to select an appropriate solvent pair. For the formation of **1**−**3**, the water−ethanol solvent pair is suitable. When the water−acetonitrile solvent pair was used, the yields of **1**−**3** were very low, and even no crystal was obtained. If the water−methanol or water−tetrahydrofuran solvent pair was selected, no product was isolated. (ii) Parallel experiments suggest that the ratio of ethanol and water also affects the formation and yields of **1**−**3**. For **1**, **2**, **3**, the optimal ratio of ethanol and water is 2:3−1:2, 1:1−1:3, 1:1−1:3, respectively. (iii) The pH is a key factor for the formation of PONs. The optimal pH is 10.1 for **1** and 10.5 for **2** and **3**.[5]

Structural Descriptions. The phase purity of **1**, **2**, and **3** was characterized by a XRPD pattern of the bulk product (Figure S1, Supporting Information). The experimental XRPD patterns of **1**−**3** are in good agreement with the simulated XRPD patterns, which indicates the phase purity of the samples. X-ray analyses reveal that **1**−**3** are all constructed from the Lindqvist anions $[Nb_6O_{19}]^{8-}$ and copper−organic complexes. **1** crystallizes in the orthorhombic space group *P*2(1)2(1)2, whereas both **2** and **3** are isostructural and belong to the orthorhombic space group *Pnnm* (Table 1). In **1**−**3**, the $[Nb_6O_{19}]^{8-}$ cluster is described as a superoctahedron of six edge-sharing NbO_6 octahedra, and the Nb−O distances can be grouped into three sets: the Nb−O_t distances are in the range of 1.761(4)−1.789(7) Å, the Nb−$O_c(\mu_6)$ distances range from 2.345(3) to 2.417(3) Å, and the Nb−O_b distances vary from 1.914(3)−2.102(7) Å (Table 3). All bond lengths are agreement with those described in the literature.[12,16,19,27] In addition, in the structural description of **1**−**3**, the Cu−O weak interactions

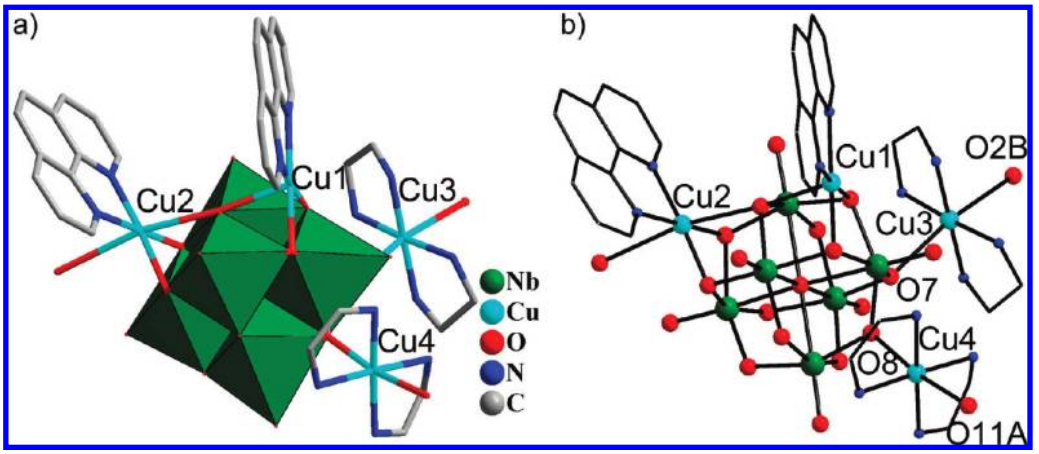

Figure 1. (a) Combined ball-and-stick/polyhedral representation of the structural unit of **1**. (b) ball-and-stick representation of the structural unit of **1**. All H atoms and crystal water molecules are omitted for clarity. The atoms with the suffixes A and B are generated by the symmetry operation: A: $-0.5-x, 0.5+y, -1-z$; B: $-0.5-x, 0.5+y, -z$.

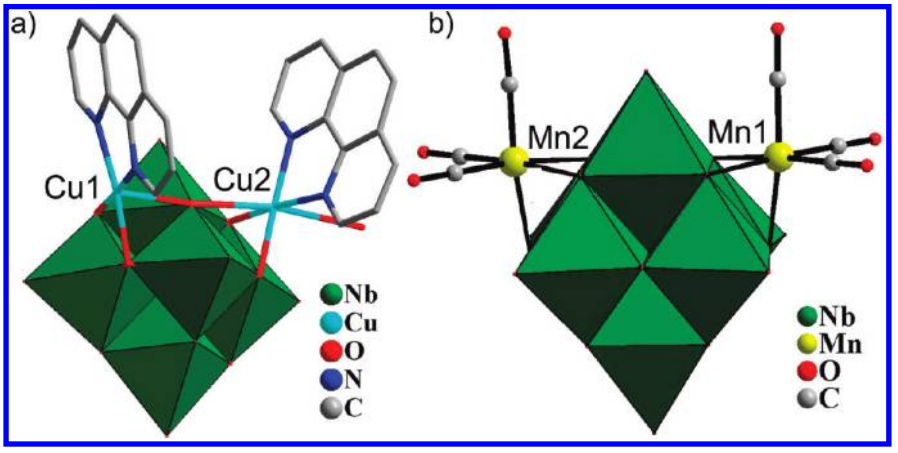

Figure 2. (a) The grafting fashion between Cu1/Cu2 complex cations and the hexaniobate anion $[Nb_6O_{19}]^{8-}$ in **1**. (b) The grafting fashion between Mn1/Mn2 complex cations and the hexaniobate anion $[Nb_6O_{19}]^{8-}$ in the reported *cis*-$K_6[\{Mn(CO)_3\}_2Nb_6O_{19}]$.

will be considered because the evident Jahn−Teller distortion of Cu^{II} ions in the crystal field leads to the elongation of the Cu−O distances.[28−30]

The structural unit of **1** consists of a hexaniobate anion $[Nb_6O_{19}]^{8-}$, a $[Cu(1,10\text{-phen})]^{2+}$, a $[Cu(1,10\text{-phen})(H_2O)]^{2+}$, and two $[Cu(en)_2]^{2+}$ cations (Figure 1). There are four crystallographically unique copper ions (Cu1, Cu2, Cu3, and Cu4) in the structural unit. The $[Cu1(1,10\text{-phen})]^{2+}$ ion is a five-coordinated square pyramid geometry, in which the basal plane is defined by two N atoms from one 1,10-phen [Cu−N: 2.000(5)−2.014(5) Å] and two μ_3−O_b atoms from one $[Nb_6O_{19}]^{8-}$ cluster [Cu−μ_3−O_b: 1.950(3)−1.969(3)] and one μ_3−O_b atom from the same $[Nb_6O_{19}]^{8-}$ cluster occupies the apical position [Cu−μ_3−O_b: 2.325(3) Å]. The $[Cu2(1,10\text{-phen})(H_2O)]^{2+}$ ion is a six-coordinated octahedral geometry with two μ_3−O_b atoms from one $[Nb_6O_{19}]^{8-}$ cluster [Cu−μ_3−O_b: 1.966(3)−1.975(3) Å] and two N atoms of one 1,10-phen building the equatorial plane [Cu−N: 2.000(5)−2.005(4) Å], and one μ_3−O_b atom from the same $[Nb_6O_{19}]^{8-}$ cluster and one coordination water O atom standing on the axial positions [Cu−μ_3−O_b: 2.447(3) Å and Cu−O_W: 2.860(6) Å]. Both $[Cu3(en)_2]^{2+}$ and $[Cu4(en)_2]^{2+}$ ions also exhibit a six-coordinated octahedral geometry achieved by four N atoms from two en [Cu−N: 1.998(5) −2.037(5) Å] and two μ_3−O_b atoms from adjacent two $[Nb_6O_{19}]^{8-}$ ions [Cu−μ_3−O_b: 2.467(3)−3.006(3) Å].

As shown in Figure 2a, both $[Cu1(1,10\text{-phen})]^{2+}$ and $[Cu2(1,10\text{-phen})(H_2O)]^{2+}$ cations are grafted on a hexaniobate anion $[Nb_6O_{19}]^{8-}$ and capped onto two adjacent $\{Nb_3O_3\}$ groups of the $[Nb_6O_{19}]^{8-}$ cluster through two stronger μ_3−O_b bridges [Cu−μ_3−O_b: 1.950(3) −1.975(3) Å] and a weak μ_3−O_b bridge [Cu−μ_3−O_b: 2.325(3)−2.447(3) Å], respectively (Figure 2a). This grafting mode between $[Cu1(1,10\text{-phen})]^{2+}$/$[Cu2(1,10\text{-phen})(H_2O)]^{2+}$ cations and the $[Nb_6O_{19}]^{8-}$ cluster is similar to that between $M(CO)_3$ cations and the $[Nb_6O_{19}]^{8-}$ cluster in $[Nb_6O_{19}\{M(CO)_3\}_n]^{(8-n)-}$ (M = Mn^I, Re^I) (Figure 2b).[11] In addition, a similar grafting mode has also been observed in polyoxotungstates.[31] Interestingly, both $[Cu1(1,10\text{-phen})]^{2+}$ and $[Cu2(1,10\text{-phen})(H_2O)]^{2+}$ cations are linked together by a common μ_3−O_b atom from the $[Nb_6O_{19}]^{8-}$ cluster with the Cu1···Cu2 distance of 4.764 Å and Cu−O−Cu angle of 173.6(1)°, forming a dicopper $[Cu_2(1,10\text{-phen})_2(H_2O)]^{4+}$ cluster. Thus, weak antiferromagnetic interactions are expected in such a system mediated by oxo-bridges. As far as we know, no organic−inorganic hybrid PON containing dicopper clusters has been reported so far.

A striking feature in **1** is that $[Cu(en)_2]_2\{[Cu(1,10\text{-phen})][Cu(1,10\text{-phen})(H_2O)]Nb_6O_{19}\}$ structural units are connected together via $[Cu4(en)_2]^{2+}$ bridges generating a novel 1D zigzag chain (Figure 3a). Such a 1D chain is somewhat different from that in $[(Nb_6O_{19}H_2)Cu(en)_2]^{4-}$ (Figure 3b).[16]

More intriguingly, adjacent 1D chains in **1** are linked to each other via O8−Cu4−O11 and O2−Cu3−O7 bridges, resulting in a 2D network structure (Figure 4a). Notably, the 2D sheet is not planar but zigzag (Figure 4b), as that occurring in $CsNa_2[\{Sn(CH_3)_2\}_3(H_2O)_4$ (β-XW_9O_{33})]·$7H_2O$ (X = As^{III}, Sb^{III}).[32] From the topological viewpoint, if each [Cu-(en)$_2$]$_2${[Cu(1,10-phen)][Cu(1,10-phen)(H_2O)]Nb_6O_{19}} unit is viewed as 4-connected node, the 2D sheet structure can be described as a (4,4)-topological network (Figure 4c). Adjacent 2D sheets are stacked in the mode of −ABAB− (Figure 4c). Although the organic−inorganic composite 2D layer architectures have been reported in polyoxotungstates,[33] to our knowledge, this topology has never been observed in PON chemistry. In addition, the packing of adjacent chains in **1** can form elliptical channels with dimensions of about 9.12 × 13.48 Å (Figure 5a,b), which are occupied by free water molecules.

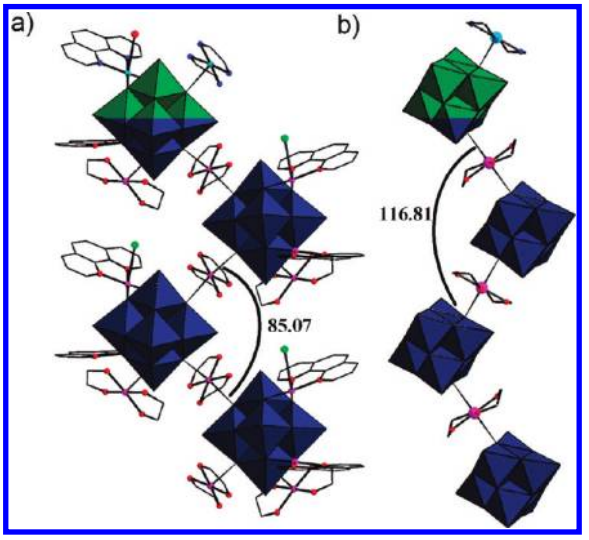

Figure 3. Comparison of the 1D chain in **1** (a) and [Cu(en)$_2$-(H_2O)$_2$]$_2$[($Nb_6O_{19}H_2$)Cu (en)$_2$]·$14H_2O$ (b).

When 2,2′-bipy and en, 2,2′-bipy and 1,2-dap were used under similar conditions, **2** and **3** were afforded, respectively. Single-crystal X-ray diffraction analyses reveal that **2** and **3** are almost isomorphic (Table 1, Figure S2, Supporting Information). Thus, only the structure of **2** is described in detail. The structural unit of **2** consists of a hexaniobate $[Nb_6O_{19}]^{8-}$ anion, one [Cu-(2,2′-bipy)]$^{2+}$ cation, one [Cu(2,2′-bipy)(H_2O)]$^{2+}$ cation, two [Cu(en)$_2$]$^{2+}$ cations, and nine lattice water molecules. Apparently, a mirror passes through the Cu1, Cu2 and the midpoint of Cu3 and Cu3A cations. As shown in Figure 6, the connection mode of the di-Cu^{II}-complex cation [Cu(2,2′-bipy)$_2$(H_2O)]$^{4+}$ with a Cu1···Cu2 distance of 4.779 Å and a Cu−O−Cu angle of 175.2(1)° is similar to that of the dimeric complex cation [Cu_2(1,10-phen)$_2$(H_2O)]$^{4+}$ in **1**. In the structural unit of **2** (Figure 6), the [Cu1(2,2′-bipy)]$^{2+}$ ion exhibits a square pyramid geometry with three μ_3−O_b atoms from one $[Nb_6O_{19}]^{8-}$ ion [Cu−μ_3−O_b: 1.965(3)−2.355(4) Å] and two N atoms from one 2,2′-bipy [Cu−N: 1.994(5) Å]. The octahedral geometry of the [Cu2(2,2′-bipy)(H_2O)]$^{2+}$ ion is defined by two N atoms from one 2,2′-bipy [Cu−N: 1.979(6) Å], one water oxygen atom [Cu−O_W: 2.969(1) Å], and three μ_3−O_b atoms from one $[Nb_6O_{19}]^{8-}$ ion [Cu−μ_3−O_b: 1.967(3)−2.428(4) Å], whereas the octahedral geometries of [Cu3(en)$_2$]$^{2+}$ and [Cu3A(en)$_2$]$^{2+}$ ions are completed by four N atoms from two en [Cu−N: 1.981(6)−2.019(6) Å] and two μ_3−O_b atoms from adjacent two $[Nb_6O_{19}]^{8-}$ ions [Cu−μ_3−O_b: 2.664(3)−2.736(3) Å].

It is noteworthy that each structural unit links to four adjacent same ones by four [Cu3(en)$_2$]$^{2+}$ bridges, generating a 2D layer in the *bc* plane (Figure 7a). Similarly, the 2D sheet of **2** is also zigzag (Figure 7b) and adopts the (4,4)-network

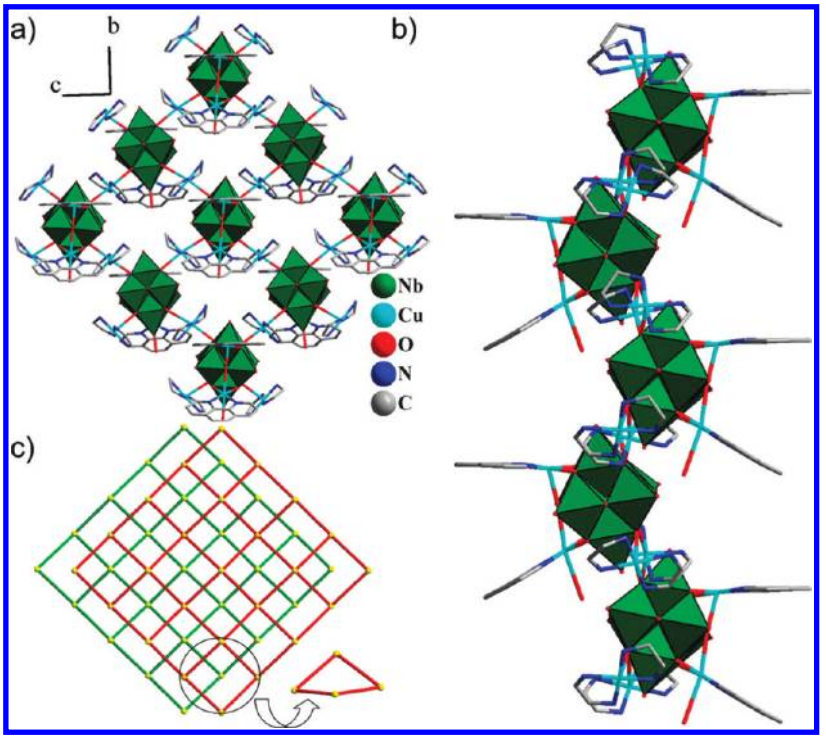

Figure 4. (a) The polyhedral/ball-and-stick view of the 2D sheet in **1**, showing one {[Cu(en)$_2$]$_2$[Cu(1,10-phen)][Cu(1,10-phen)(H_2O)]Nb_6O_{19}} structural unit connecting four [Cu(en)$_2$]$^{2+}$ bridging groups. (b) Side view of the 2D solid-state structure of **1**. (c) The 2D (4,4) topological network of **1** viewed along the *a* direction. Yellow balls are the four-connected nodes and represent the [Cu(en)$_2$]$_2${[Cu(1,10-phen)][Cu(1,10-phen) (H_2O)]Nb_6O_{19}} units. H atoms and lattice water molecules have been omitted for clarity.

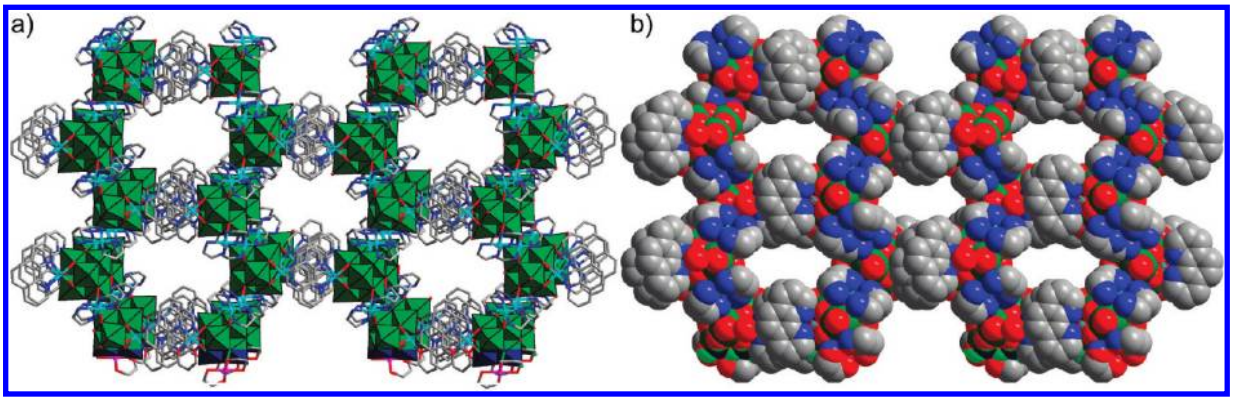

Figure 5. (a, b) Packing representations of **1** along the *b* axis. The lattice water molecules have been omitted for clarity.

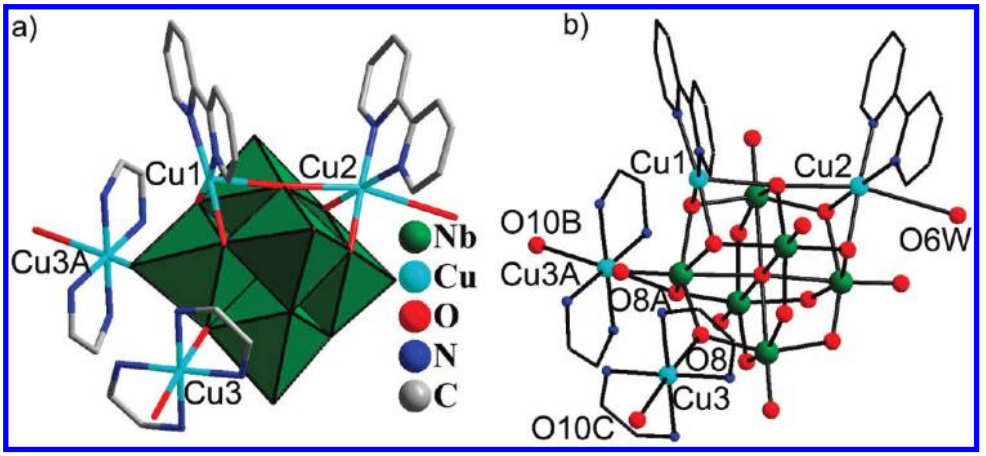

Figure 6. (a) Combined ball-and-stick/polyhedral representation of the structural unit of **2**. (b) ball-and-stick representation of the structural unit of **2**. All H atoms and crystalline water molecules are omitted for clarity. The atoms with the suffixes A, B and C are generated by the symmetry operation: A: $x, y, -z$; B: $0.5-x, -0.5+y, -0.5+z$; C: $0.5-x, -0.5+y, 0.5-z$.

topology (Figure 7c), in which each $[Cu(en)_2]_2\{[Cu(2,2'\text{-bpy})][Cu(2,2'\text{-bpy})(H_2O)]Nb_6O_{19}\}$ unit serves as a four-connected node. In addition, the packing of **2** and **3** exhibits elliptical channels along the *b* axis with dimensions of about 9.21 × 5.38 Å for **2** (Figure 7d) and 7.78 × 5.12 Å for **3**, respectively. Free water molecules reside in the channels, which is analogous to that in **1**.

1−**3** represent the first examples of organic−inorganic hybrid hexaniobates containing aliphatic and aromatic N-ligands. Furthermore, **1**−**3** show a rare 2D zigzag structure with a (4,4)-topological network in PON chemistry, which obviously differs from the previous PONs with discrete or 1D structures.[7,9,11,16] Though the structure of **1** is similar to that of **2**−**3**, there are still some differences between them: (1) **2** and **3** crystallize in the orthorhombic space group *Pnnm*, whereas **1** belongs to the orthorhombic space group *P*2(1)2(1)2. (2) There is a mirror passing through the structural unit in **2** or **3**; in contrast, no mirror exists in the structural unit of **1**. (3) There are three crystallographically unique Cu^{II} ions in **2**−**3**, while four crystallographically unique Cu^{II} ions exist in **1**. (4) The structural units of **2** and **3** are linked by $[Cu3(en)_2]^{2+}$ bridges, generating a 2D sheet, while the structural units of **1** are connected by the $[Cu3(en)_2]^{2+}$ and $[Cu4(en)_2]^{2+}$ bridges. From the above analyses, we presume that the steric constraints imposed by the 2,2′-bipy ligand are quite different from those of the 1,10-phen,[34] leading to the structural differences for **2**−**3** and **1**.

FT-IR and UV Spectroscopy. In the IR spectra, the bands in the 400−1000 cm^{-1} region exhibit similar characteristic vibration patterns derived from the Lindqvist-type polyoxoanions (Figure S3, Supporting Information). The $\nu(Nb-O_t)$ characteristic band appears at 854 cm^{-1} for **1**, 851 cm^{-1} for **2**, and 858 cm^{-1} for **3**, respectively. Their $\nu(Nb-O_b)$ vibration frequencies in the region of 400−800 cm^{-1} show evident red shifts compared with that of the precursor $K_7HNb_6O_{19}\cdot 13H_2O$, which suggests that the transition-metal cations have coordinated to PONs.[18] In the IR spectrum of **1**, the occurrence of the stretching (3324−3235 cm^{-1}) and bending (1584 cm^{-1}) bands of $-NH_2$ group confirms the presence of en ligands. The vibration bands ranging from 1398 to 1518 cm^{-1} are attributed to the 1,10-phen group.[35] In the IR spectrum of **2**, the stretching and bending bands of the $-NH_2$ group appear at 3299−3138 cm^{-1} and 1604 cm^{-1}, respectively, corresponding to the presence of en ligands. The vibration peaks between 1495 and 1448 cm^{-1} result from the 2,2′-bipy group.[33c,34] In the IR spectrum of **3**, similar characteristic absorption bands of 2,2′-bipy have been observed. The stretching and bending bands of $-NH_2$ groups appear at 3258−3134 cm^{-1} and 1602 cm^{-1}, respectively, indicating the presence of dap ligands. All the characteristic peaks are consistent with the results of single-crystal X-ray diffraction analyses. The UV spectra of **1** and **2** in aqueous solution were recorded at pH = 7.0 and 7.4, respectively. There are two characteristic absorption peaks at approximately 222 and 272 nm for **1**, 224, 301 nm for **2**, respectively. The higher energy band (222 and 224 nm) can be attributed to the charge-transfer transitions of the O → Nb bond in comparison with the $[Nb_6O_{19}]^{8-}$ anion (Figure 8), whereas the lower energy

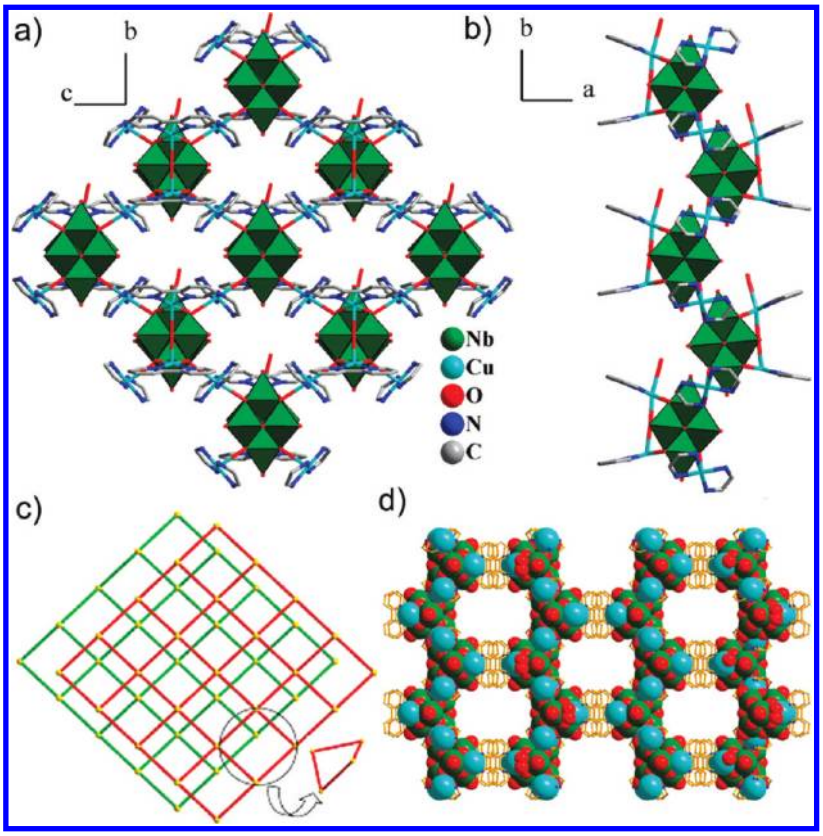

Figure 7. (a) The polyhedral/ball-and-stick view of the 2D sheet structure of **2** showing the $\{[Cu(en)_2]_2[Cu(2,2'\text{-bipy})][Cu(2,2'\text{-bipy})(H_2O)]Nb_6O_{19}\}$ structural units interconnected through $[Cu(en)_2]^{2+}$ bridges along the *a* direction. (b) Side view of the 2D sheet of **2**. (c) The 2D (4,4) topological network of **2** viewed along the *a* direction. Yellow balls are the four-connected nodes and represent the $\{[Cu(en)_2]_2[Cu(2,2'\text{-bipy})][Cu(2,2'\text{-bipy})(H_2O)]Nb_6O_{19}\}$ units. (d) View of the crystal packing of **2** along the *b* axis. H atoms and lattice water molecules have been omitted for clarity.

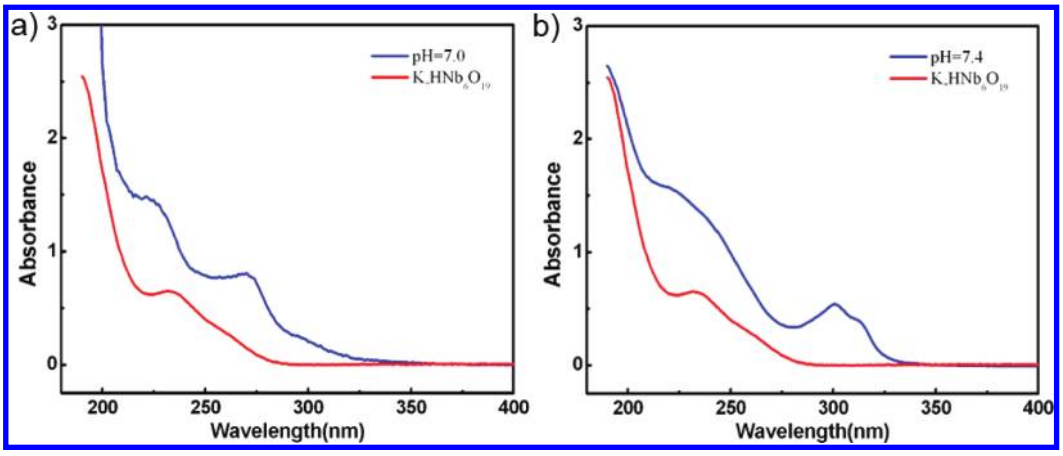

Figure 8. (a) Comparison of the UV spectra of **1** (pH = 7.0) and $K_7HNb_6O_{19}$. (b) Comparison of the UV spectra of **2** (pH = 7.4) and $K_7HNb_6O_{19}$.

band (273 and 301 nm) should correspond to ligand-to-metal (Cu^{II}) charge transfer (LMCT) transitions.[36]

TG Analyses. The thermal stability of **1**−**3** (Figure 9) was investigated on crystalline samples under air atmosphere from 25 to 800 °C. The TG curves of **1**−**3** all exhibit two steps of weight loss. In **1**, the first weight loss of 10.37% between 25 and 131 °C is assigned to the release of 10 and a half lattice water molecules (calcd. 9.83%). Followed by a weight loss of 31.47% approximately between 221 and 800 °C corresponds to the removal of four en ligands, two 1,10-phen ligands, and one coordinated water molecule (calcd. 34.02%). The whole weight loss of 41.84% is consistent with the calculated value of 43.85%. For **2**, the first weight loss of 9.36% from 25 to 112 °C corresponds to the loss of nine lattice water molecules (calcd. 8.77%). On further heating, the second weight loss of 27.73% from 210 to 800 °C comes from the removal of four en ligands, two 2,2′-bipy ligands, and one coordinated water molecule (calcd. 30.88%). It shows a total weight loss of 37.09% in the range of 25−800 °C, which agrees well with the calculated value of 39.65%. In the case of **3**, the first weight loss of 10.70% from 25 to 131 °C involves the loss of 11 lattice water molecules (calcd. 10.19%), and the second weight loss of 32.39% from 212 to 800 °C results from the release of four 1,2-dap ligands, two 2,2′-bipy ligands, and one coordinated water molecule (calcd. 32.24%). It shows a total weight loss of 43.09% in the range of 25−800 °C, which is consistent with the calculated value of 42.43%.

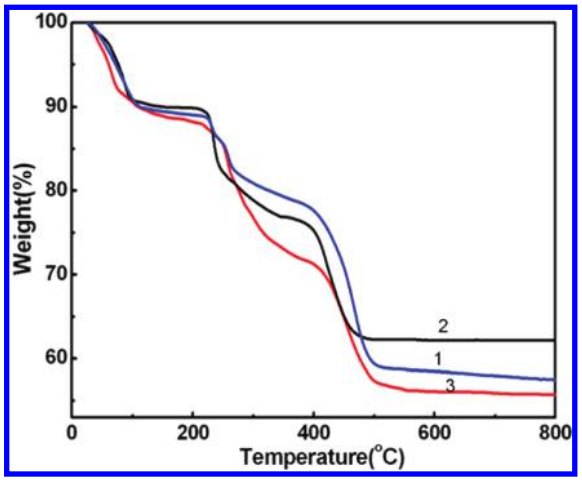

Figure 9. The TG curves of **1**−**3** on crystalline samples in an air atmosphere in the range of 25−800 °C.

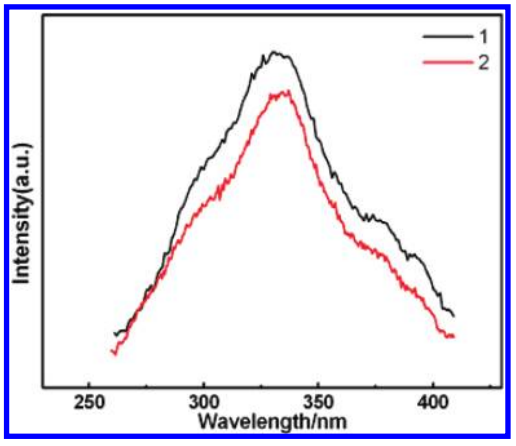

Figure 10. Solid-state emission spectra of **1** and **2** at room temperature.

Photoluminescence. Considerable interest in organic−inorganic hybrids photoluminescence materials has been developed due to their potential applications in lighting, analytical probes, and lasers.[37] The solid-state luminescence properties of **1**, **2**, and $K_7HNb_6O_{19}\cdot 13H_2O$ were investigated at room temperature. The emission spectra of **1** and **2** are depicted in Figure 10. It can be observed that **1** displays intense emission band at ca. 330 nm upon excitation at 227 nm. To understand the nature of the emission band, the solid-state luminescence emission of the free 1,10-phen ligand was investigated upon excitation at 227 nm. Two obvious emissions at 362 and 380 nm are observed for free 1,10-phen ligand (Figure S4a, Supporting Information).[35,38] In addition, the hexaniobate $K_7HNb_6O_{19}\cdot 13H_2O$ displays a broad emission band at around 320 nm in the visible region upon excitation at 227 nm (Figure S4a, Supporting Information), which can be attributed to the O → Nb charge transfer.[39] Thus, the emission of **1** may be assigned to the mixture of the intraligand $\pi_L^*-\pi_L$ transitions from the 1,10-phen and the O → Nb charge transfer of $K_7HNb_6O_{19}\cdot 13H_2O$.[35,39] Upon excitation at 225 nm, **2** exhibits emission band maxima at ca. 336 nm with a weaker intensity than that of **1**. Notably, the excitation spectra of **1** and **2** resemble each other in the peak profile. Additionally, the free 2,2′-bipy ligand displays weak luminescence at ca. 360 nm upon excitation at 230 nm (Figure S4b, Supporting Information).[35] Therefore, we speculate that the emission of **2** also arises from the intraligand $\pi_L^*-\pi_L$ transitions and the O → Nb transitions of $K_7HNb_6O_{19}\cdot 13H_2O$. These results indicate that **1**−**3** may be applicable as potential photoactive materials.

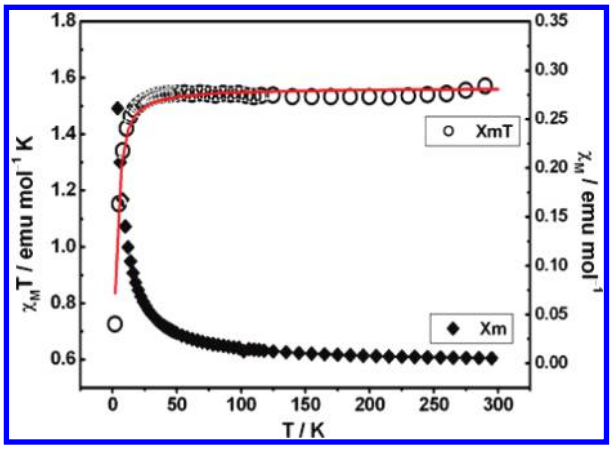

Figure 11. The plots of χ_M and $\chi_M T$ vs T in the temperature of 2−300 K for **1**. The red solid line represents the fit to experimental data.

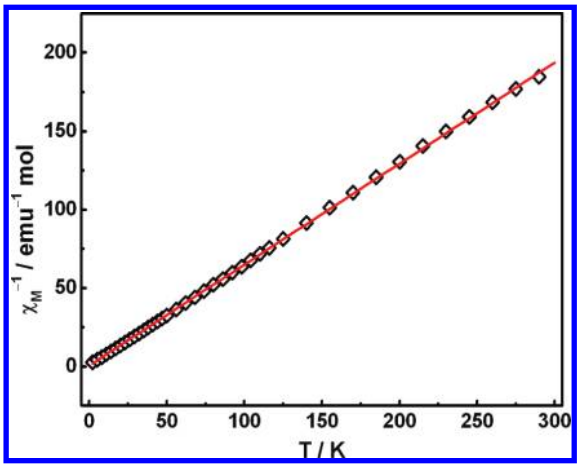

Figure 12. The temperature evolution of the inverse magnetic susceptibility χ_M^{-1} between 4 and 300 K for **1**.

Magnetic Properties. Considering the similarity of **1**, **2**, and **3** in structure, only the magnetic behavior of **1** was investigated. The temperature dependence of magnetic susceptibility for **1** is shown in Figure 11 in the form of χ_M and $\chi_M T$ versus T. The χ_M slowly increases from 0.006 emu mol^{-1} at 300 K to 0.031 emu mol^{-1} at 50 K and then exponentially reaches the maximum of 0.36 emu mol^{-1} at 2 K. The $\chi_M T$ product at room temperature is 1.58 emu mol^{-1} K, being consistent with the expected spin-only value (1.5 emu mol^{-1} K) for four isolated Cu^{II} ions assuming $g = 2.00$. On cooling, the $\chi_M T = f(T)$ curve decreases to a minimum of 0.73 emu mol^{-1} K at 2 K, indicating the antiferromagentic interactions between the Cu^{II} centers. Fit the magnetic susceptibility data between 2 and 300 K to the Curie−Weiss expression affording the Curie constant $C = 1.55$ emu mol^{-1} K and the Weiss constant $\theta = -0.93$ K (Figure 12). The small negative Weiss constant also manifests the occurrence of weak antiferromagnetic interactions within Cu^{II} centers.

As seen from the structure of **1**, a binuclear Cu^{II} unit with the Cu1···Cu2 distance of 4.764 Å is included in **1**. Accordingly, the magnetic susceptibility data can be fitted to the modified Bleaney−Bowers equation derived from the Hamiltonian $H = -J\tilde{S}_1\tilde{S}_2$ for the binuclear Cu^{II} entity.[40,41] Considering the paramagnetic $[Cu3(en)_2]^{2+}$ and $[Cu4(en)_2]^{2+}$ cations, the expression

of molar magnetic susceptibility of **1** is written as follows:[42]

$$\chi_M = (1-\rho)\frac{2Ng^2\beta^2}{kT} \times \frac{1}{3+e^{-2J/kT}} + \frac{Ng^2\beta^2}{2kT}\rho + \frac{Ng^2\beta^2}{3kT} \times 2 \quad (1)$$

Here, J is the exchange constant within the dinuclear Cu^{II} cluster, N is the Avogadro number, ρ is the fraction of paramagnetic impurity in the sample, g is the Landé g factor, β is the electronic Bohr magneton, and k is the Boltzmann constant.

The best-fit parameters obtained in the overall temperature range are $J = -2.80\ cm^{-1}$, $g = 2.04$, and $\rho = 5\times10^{-4}$. The negative J value further confirms the presence of the weak antiferromagnetic interactions in **1**. Such antiferromagnetic coupling in the dinuclear Cu^{II} cluster units has been observed in $[Cu_2(bzacpro)\ (CH_3CO_2)]$\{($H_3$bzacpro = *N*,*N*′-bis(1-methyl-3-hydroxy-3-phenyl-2-propen-1-ylidene-1,3-diamino-2-propanol)\},[43] $[Na_{12}(H_2O)_{36}][Cu_2(\beta\text{-Y-}GeMo_9O_{33})_2]\cdot 3H_2O$,[40] and $\{[Cu_5(2,2'\text{-bipy})_5(H_2O)][GeW_9O_{34}]\}_2\cdot 7H_2O$.[31b] Besides, similar antiferromagnetic coupling is also observed in tri-, tetra-, and high-nuclear Cu^{II} cluster.[33c,43,44] Furthermore, it is well-known from previous studies the correlation within the oxo-bridged dinuclear Cu(II) units between J and the Cu−O−Cu angle: an antiferromagnetic exchange interaction is found when the Cu−O−Cu bond angle is larger than 98°, while the Cu−O−Cu bond angle smaller than 98° can facilitate the ferromagnetic exchange interaction.[45,46] In the case of **1**, because the Cu−O−Cu angle is 173.6(1)°, the antiferromagnetic interaction within Cu^{II} ions is expected, which is in accordance with the simulated result. Notably, the Cu−O−Cu angle of 173.6(1)° in **1** is much larger than those in the reported antiferromagnetic oxo-bridged dinuclear Cu^{II} compounds $[Cu_2(bzacpro)\ (CH_3CO_2)]$ (131.8(3)°),[43] $[Cu_2(bzacbu)(CH_3CO_2)]$ (125.1(4) and 125.3(3)°) {(bzacbu = *N*,*N*′-bis(1-methyl-3-hydroxy-3-phenyl-2-propen-1-ylidene-1,4-diamino-2-butanol)\},[43] $[Cu_2(L)(H_2O)_2]F_2(CH_3OH)_2$(103.65(10)°) (L = 4-Methyl-2,6-diformylphenol),[47] $[Cu(2,2'\text{-bipy})\ (H_2O)][H_2PW_{11}O_{39}Cu_2(2,2'\text{-bipy})_2(H_2O)(OH)]\cdot 1.5H_2O$ (122.3°).[48]

Conclusions

Three novel organic−inorganic hybrid PONs: $[Cu(en)_2]_2\{[Cu(phen)][Cu(phen)(H_2O)]Nb_6O_{19}\}\cdot 10.5\ H_2O$ (**1**), $[Cu(en)_2]_2\{[Cu(2,2'\text{-bipy})][Cu(2,2'\text{-bipy})(H_2O)]\ Nb_6O_{19}\}\cdot 9H_2O$ (**2**), and $[Cu(1,2\text{-dap})_2]_2\{[Cu(2,2'\text{-bipy})]\ [Cu(2,2'\text{-bipy})(H_2O)]Nb_6O_{19}\}\cdot 11H_2O$ (**3**) have been synthesized by the solution-diffusion method rather than the evaporation or hydrothermal technique. These findings have three major features: (i) we utilize the rare solution−diffusion method in PON chemistry to prepare organic−inorganic hybrid PON-based extended frameworks; (ii) **1**−**3** are the first examples of Lindqvist-type hexaniobates with mixed organic ligands; (iii) **1**−**3** represent the first examples of 2D architecture with a (4,4)-connected topology network. In the following work, we will introduce some functional N-heterocyclic aromatic polycarboxylate ligands to the present system to construct more high-dimensional organic−inorganic hybrid Lindqvist-templated PONs with mixed organic ligands. In addition, we are trying to synthesize organic−inorganic hybrid 3d-4f heterobimetal PONs.

Acknowledgment. This work was supported by the Natural Science Foundation of China, Special Research Fund for the Doctoral Program of Higher Education, Innovation Scientists and Technicians Troop Construction Projects of Henan Province, the Foundation of Education Department of Henan Province and Natural Science Foundation of Henan Province.

Supporting Information Available: X-ray crystallographic files for **1**−**3** in CIF format and additional figures. This material is available free of charge via the Internet at http://pubs.acs.org.

References

(1) (a) Long, D. L.; Tsunashima, R.; Cronin, L. *Angew. Chem., Int. Ed.* **2010**, *49*, 1736–1758. (b) Song, Y. F.; Long, D. L.; Cronin, L. *Angew. Chem., Int. Ed.* **2007**, *46*, 3900–3904. (c) Bassil, B. S.; Dickman, M. H.; Römer, I.; Kammer, B.v.d.; Kortz, U. *Angew. Chem., Int. Ed.* **2007**, *46*, 6192–6195. (d) Sadakane, M.; Dickman, M. H.; Pope, M. T. *Angew. Chem., Int. Ed.* **2000**, *39*, 2914–2916. (e) Finn, R. C.; Burkholder, E.; Zubieta, J. *Chem. Commun.* **2001**, 1852–1853. (f) Wang, X. L.; Qin, C.; Wang, E. B.; Su, Z. M.; Li, Y. G.; Xu, L. *Angew. Chem., Int. Ed.* **2006**, *45*, 7411–7414. (g) Liu, S. X.; Xie, L. H.; Gao, B.; Zhang, C. D.; Sun, C. Y.; Li, D. H.; Li, D. H.; Su, Z. M. *Chem. Commun.* **2005**, 5023–5025. (h) Wang, J. P.; Zhao, J, W.; Duan, X. Y. *Cryst. Growth Des.* **2006**, *6*, 507–513. (i) Müller, A.; Reuter, H.; Dillinger, S. *Angew. Chem., Int. Ed.* **1995**, *34*, 2328–2361.

(2) (a) Hagrman, P. J.; Hagrman, D; Zubieta, J. *Angew. Chem., Int. Ed.* **1999**, *38*, 2638–2684. (b) Bareyt, S.; Piligkos, S.; Hasenknopf, B.; Gouzerh, P.; Lacote, E.; Thorimbert, S.; Malacria, M. *J. Am. Chem. Soc.* **2005**, *127*, 6788–6794. (c) An, H. Y.; Wang, E. B.; Xiao, D. R.; Li, Y. G.; Su, Z. M.; Xu, L. *Angew. Chem., Int. Ed.* **2006**, *45*, 904–908. (d) Pope, M. T.; Müller, A. *Angew. Chem., Int. Ed.* **1991**, *30*, 34–48. (e) Ren, Y. P.; Kong, X. J.; Hu, X. Y.; Sun, M.; Long, L. S.; Huang, R. B.; Zheng, L. S. *Inorg. Chem.* **2006**, *45*, 4016–4023. (f) Cao, R. G.; Liu, S. X.; Xie, L. H.; Pan, Y. B.; Cao, J. F.; Ren, Y. H.; Xu, L. *Inorg. Chem.* **2007**, *46*, 3541–3547. (g) Fan, D. W.; Jia, X. F.; Tang, P. Q.; Hao, J. C.; Liu, T, B. *Angew. Chem., Int. Ed.* **2007**, *46*, 3342–3345.

(3) (a) Hagrman, D.; Hagrman, P. J.; Zubieta, J. *Angew. Chem., Int. Ed.* **1999**, *38*, 3165–3168. (b) Kumar, D.; Derat, E.; Khenkin, A. M.; Neumann, R.; Shaik, S. *J. Am. Chem. Soc.* **2005**, *127*, 17712–17718. (c) Rhule, J. T.; Neiwert, W. A.; Hardcastle, K. I.; Do, B. T.; Hill, C. L. *J. Am. Chem. Soc.* **2001**, *123*, 12101–12102. (d) Yamase, T.; Fukaya, K.; Nojiri, H.; Ohshima, Y. *Inorg. Chem.* **2006**, *45*, 7698–7704. (e) Ishii, Y.; Takenaka, Y.; Konishi, K. *Angew. Chem., Int. Ed.* **2004**, *43*, 2702–2705.

(4) Lindqvist, I. *Ark. Kemi* **1953**, *5*, 247–250.

(5) Bontchev, R. P.; Nyman, M. *Angew. Chem., Int. Ed.* **2006**, *45*, 6670–6672.

(6) Tsunashima, R.; Long, D. L.; Miras, H. N.; Gabb, D.; Pradeep, C. P.; Cronin, L. *Angew. Chem., Int. Ed.* **2009**, *48*, 113–117.

(7) Flynn, C. M.; Stucky, G. D. *Inorg. Chem.* **1969**, *8*, 332–335.

(8) Graeber, E. J.; Morosin, B. *Acta Crystallogr. Sect. B* **1977**, *33*, 2137–2143.

(9) Yamase, T.; Naruke, H.; Sasaki, Y. *Inorg. Chem.* **1994**, *33*, 409–410.

(10) (a) Rhule, J. T.; Hill, C. L.; Judd, D. A. *Chem. Rev.* **1998**, *98*, 327–358. (b) Chiang, M. H.; Williams, C. W.; Soderhlm, L.; Antonio, M. R. *Eur. J. Inorg. Chem.* **2003**, *14*, 2663–2669. (c) Russell, A. J.; Berberich, J. A.; Drevon, G. F.; Koepsel, R. R. *Annu. Rev. Biomed. Eng.* **2003**, *5*, 1–27. (d) Kortz, U.; Savelieff, M. G.; Bassil, B. S.; Keita, B.; Nadjo, L. *Inorg. Chem.* **2002**, *41*, 783–789.

(11) Besserguenev, A.; Dickman, M.; Pope, M. *Inorg. Chem.* **2001**, *40*, 2582–2586.

(12) Hegetschweiler, K.; Finn, R.; Rarig, R.; Sander, J.; Steinhauser, S.; Wörle, M.; Zubieta, J. *Inorg. Chim. Acta* **2002**, *337*, 39–47.

(13) (a) Nyman, M.; Bonhomme, F.; Alam, T. M.; Rodriguez., M. A.; Cherry, B. R.; Krumhansl, J. L.; Nenoff, T. M.; Sattler, A. M. *Science* **2002**, *297*, 996–998. (b) Nyman, M.; Bonhomme, F.; Alam, T. M.; Parise, J. B.; Vaughan, G. M. B. *Angew. Chem., Int. Ed.* **2004**, *43*, 2787–2792. (c) Bonhomme, F.; Larentzos, J. P.; Alam, T. M.; Maginn, E. J.; Nyman, M. *Inorg. Chem.* **2005**, *44*, 1774–1785.

(14) Nyman, M.; Celestian, A. J.; Parise, J. B.; Holland, G. P.; Alam, T. M. *Inorg. Chem.* **2006**, *45*, 1043–1052.

(15) Maekawa, M.; Ozawa, Y.; Yagasaki, A. *Inorg. Chem.* **2006**, *45*, 9608–9609.

(16) Bontchev, R. P.; Venturini, E. L.; Nyman, M. *Inorg. Chem.* **2007**, *46*, 4483–4491.

(17) (a) Villa, E. M.; Ohlin, C. A.; Balogh, E.; Anderson, T. M.; Nyman, M. D.; Casey, W. H. *Angew. Chem., Int. Ed.* **2008**, *47*, 4844–4846. (b) Ohlin, C. A.; Villa, E. M.; Casey, W. H. *Inorg. Chim. Acta* **2009**, *362*, 1391–1392.

(18) Niu, J. Y.; Ma, P. T.; Niu, H. Y.; Li, J.; Zhao, J. W.; Song, Y.; Wang, J. P. *Chem.—Eur. J.* **2007**, *13*, 8739–8748.
(19) Wang, J. P.; Niu, H. Y.; Niu, J. Y. *Inorg. Chem. commun.* **2008**, *11*, 63–65.
(20) Shen, L.; Li, C. H.; Chi, Y. N.; Hu, C. W. *Inorg. Chem. Commun.* **2008**, *11*, 992–994.
(21) Filowitz, M.; Ho, R. K. C.; Klemperer, W. G.; Shum, W. *Inorg. Chem.* **1979**, *18*, 93–103.
(22) (a) Sheldrick, G. M. *SHELXS97, Program for Crystal Structure Solution*; University of Göttingen: Göttingen, Germany, 1997; (b) Sheldrick, G. M. *SHELXL97, Program for Crystal Structure Refinement*; University of Göttingen: Germany, 1997.
(23) Niu, J. Y.; Chen, G.; Zhao, J. W.; Ma, P. T.; Li, S. Z.; Wang, J. P.; Li, M. X.; Bai, Y.; Ji. B. S. *Chem. Eur. J.* **2010**, DOI: 10.1002/chem.201000824.
(24) (a) Alam, T. M.; Nyman, M.; Cherry, B. R.; Segall, J. M.; Lybarger, L. E. *J. Am. Chem. Soc.* **2004**, *126*, 5610–5620. (b) Nyman, M.; Alam, T.; Bonhomme, F.; Rodriguez, M.; Frazer, C.; Welk, M. *J. Cluster Sci.* **2006**, *17*, 197–219.
(25) Ren, Y. P.; Kong, X. J.; Hu, X. Y.; Sun, M.; Long, L. S. *Inorg. Chem.* **2006**, *45*, 4016–4024.
(26) (a) Burkholder, E.; Wright, S.; Golub, V.; ÓConnor, C. J.; Zubieta, J. *Inorg. Chem.* **2003**, *42*, 7460–7471. (b) Lisnard, L.; Dolbecq, A.; Mialane, P.; Marrot, J.; Codjovi, E.; Sécheresse, F. *Dalton Trans.* **2005**, 3913–3920.
(27) Anderson, T. M.; Thoma, S. G.; Bonhomme, F.; Rodriguez, M. A; Park, H.; Parise, J. B.; Alam, T. M.; Larentzos, J. P.; Nyman, M. *Cryst. Growth. Des.* **2007**, *7*, 719–723.
(28) Burkholder, E.; Zubieta, J. *Chem. Commun.* **2001**, 2056–2057.
(29) (a) Cao, R. G.; Liu, S. X.; Xie, L. H.; Pan, Y. B.; Cao, J. F.; Ren, Y. H.; Xu, L. *Inorg. Chem.* **2007**, *46*, 3541–3547. (b) Reinoso, S.; Vitoria, P.; Lezama, L.; Luque, A.; Gutiérrez-Zorrilla, J. M. *Inorg. Chem.* **2003**, *42*, 3709–3711.
(30) Billing, D. E.; Hathaway, B. J.; Nivholls, P. J. J. *Chem. Soc. A.* **1970**, 1877–1881.
(31) (a) Wang, J. P.; Ma, P. T.; L, J.; Niu, J. Y. *Chem. Lett.* **2006**, *35*, 994–995. (b) Wang, C. M.; Zheng, S. T.; Yang, G. Y. *Inorg. Chem.* **2007**, *46*, 616–618.
(32) Hussain, F.; Reicke, M.; Kortz, U. *Eur. J. Inorg. Chem.* **2004**, 2733–2738.
(33) (a) Zhang, Z. M.; Liu, J.; Wang, E. B.; Qin, C.; Li, Y. G.; Qi, Y. F.; Wang, X. L. *Dalton Trans.* **2008**, 463–468. (b) Zhao, J. W.; Li, B.; Zheng, S. T.; Yang, G. Y. *Cryst. Growth. Des.* **2007**, *7*, 2658–2664. (c) Zhao, J. W.; Wang, C. M.; Zhang, J.; Zheng, S. T.; Yang, G. Y. *Chem.—Eur. J.* **2008**, *14*, 9223–9239.
(34) Yuan, M.; Li, Y. G.; Wang, E. B.; Tian, C. G.; Wang, L.; Hu, C. W.; Hu, N. H.; Jia, H. Q. *Inorg. Chem.* **2003**, *42*, 3670–3676.
(35) Sun, C. Y.; Li, Y. G.; Wang, E. B.; Xiao, D. G.; An, H. Y.; Xu., L. *Inorg. Chem.* **2007**, *46*, 1563–1574.
(36) Yu, K.; Li, Y. G.; Zhou, B. B.; Su, Z. H.; Zhao, Z. F.; Zhang, Y. N. *Eur. J. Inorg. Chem.* **2007**, 5662–5669.
(37) (a) Würthner, F.; Sautter, A. *Chem. Commun.* **2000**, 445. (b) Ciurtin, D. M.; Pschirer, N. G.; Smith, M. D.; Bunz, U. H. F.; zur Loye, H. C. *Chem. Mater.* **2001**, *13*, 2743–2745. (c) Tao, J.; Shi, J. X.; Tong, M. L.; Zhang, X. X.; Chen, X. M. *Inorg. Chem.* **2001**, *40*, 6328–6330.
(38) Du, Z. Y.; Li, X. L.; Liu, Q. Y.; Mao, J. G. *Cryst. Growth Des.* **2007**, *7*, 1501–1507.
(39) Blasse, G.; Grabmaier, B. C. *Luminescence Materials*; Springer-Verlag: New York, 1994.
(40) Li, S. Z.; Zhao, J. W.; Ma, P. T.; Du, J.; Niu, J. Y.; Wang, J. P. *Inorg. Chem.* **2009**, *48*, 9819–9830.
(41) Koner, S.; Saha, S.; Mallah, T.; Okamoto, K. I. *Inorg. Chem.* **2004**, *43*, 840–842.
(42) Kahn, O. *Molecular Magnetism*; VCH Publishers: New York, 1993, p 132.
(43) Mikuriya, M.; Minowa, K.; Nukada, R. *Bull. Chem. Soc. Jpn.* **2002**, *75*, 2595–2607.
(44) (a) Liu, J. C.; Guo, G. C.; Huang, J. S.; You, X. Z. *Inorg. Chem.* **2003**, *42*, 235–243. (b) Liu, H.; Qin, C.; Wei, Y. G.; Xu, L.; Gao, G. G.; Li, F. Y.; Qu, X. S. *Inorg. Chem.* **2008**, *47*, 4166–4172.
(45) (a) Ruiz, E.; Alemany, P.; Alvarez, S.; Cano, J. *J. Am. Chem. Soc.* **1997**, *119*, 1297–1303. (b) Aromí, G.; Ribas, J.; Gamez, P.; Roubeau, O.; Kooijman, H.; Spek, A. L.; Teat, S.; MacLean, E.; Stoeckli-Evans, H.; Reedijk, J. *Chem.—Eur. J.* **2004**, *10*, 6476–6488. (c) Shores, M. P.; Bartlett, B. M.; Nocera, D. G. *J. Am. Chem. Soc.* **2005**, *127*, 17986–17987.
(46) (a) Liu, H.; Qin, C.; Wei, Y. G.; Xu, L.; Gao, G. G.; Li, F. Y.; Qu, X. S. *Inorg. Chem.* **2008**, *47*, 4166–4172. (b) Liu, H. S.; Gómez-García, C. J.; Peng, J.; Feng, Y. H.; Su, Z. M.; Sha, J. Q.; Wang, L. X. *Inorg. Chem.* **2007**, *46*, 10041–10043.
(47) Thompson, L. K.; Mandal, S. K.; Tandon, S. S.; Bridson, J. N.; Park, M. K. *Inorg. Chem.* **1996**, *35*, 3117–3125.
(48) Li, B.; Zhao, J. W.; Zheng, S. T.; Yang, G. Y. *Inorg. Chem. Commun.* **2008**, *11*, 1288–1291.